https://doi.org/10.5194/nhess-2020-322
Preprint. Discussion started: 6 October 2020
© Author(s) 2020. CC BY 4.0 License.

Natural Hazards and Earth System Sciences
Discussions

Assessing the effect of lithological setting, block characteristic and slope topography on the runout length of rockfalls in the Alps and on the La Réunion island

Kerstin Wegner[1], Florian Haas[1], Tobias Heckmann[1], Anne Mangeney[2], Virginie Durand[2,a], Nicolas Villeneuve[2,3], Philippe Kowalski[2,4], Aline Peltier[2,4], Michael Becht[1]

[1]Chair of Physical Geography, Catholic University of Eichstaett-Ingolstadt, Eichstaett, 85072, Germany
[2]Université de Paris, Institut de Physique du Globe de Paris, CNRS, F-75005 Paris, France
[3]Université de La Réunion, Laboratoire Géosciences Réunion, F-97744 Saint Denis, France
[4]Observatoire Volcanologique du Piton de la Fournaise, Institut de Physique du Globe de Paris, F-97418 La Plaine des Cafres, France
[a]now at: Helmholtz Centre Potsdam German Research Centre for Geosciences, GFZ, 14473 Potsdam, Germany

Correspondence to: Kerstin Wegner (KWegner@ku.de)

Abstract. In high mountain regions, rockfalls are common processes, which transport different volumes of material and therefore endanger populated areas and infrastructure facilities. In four study areas within different lithological settings, LiDAR (light detection and ranging) data were acquired for a morphometric analysis of block sizes, block shapes and talus cone characteristics. Based on these high-resolution terrestrial laser scanning (TLS) data, the three axes of every block larger than 0.5 m in the referenced point cloud were measured. Block sizes and shapes are used to investigate them in the context of runout distances and to analyse the spatial distribution of blocks on the talus cone. We also investigate the influence of terrain parameters such as slope inclination, roughness and profile curvature (longitudinal profiles). Our study shows that the relation of block size within different lithological settings on runout length is complex, because we can neither confirm nor reject the theory of gravitational sorting. We also found that the block shape (axial ratio) does not have a simple influence on runout length, as it plays the role of a moderating parameter in two study sites (Gampenalm: GA, Dreitorspitze: DTS) while we could not confirm this for Piton de la Fournaise (PF) and Zwieselbach valley (ZBT). The derived roughness values show a clear difference between the four study sites. This also applies for the parameter of slope inclination and longitudinal profiles.

1. Introduction

Rockfall is an important geomorphic process on steep rock slopes and thus plays a significant role for the geomorphic dynamics especially in high mountainous regions (e.g. Hungr and Evans, 1988, Krautblatter and Dikau, 2007, Bennett, et al., 2012, Frattini et al., 2012). Rock fragments are detached from cliff faces (primary rockfall) or remobilized from sediment stores (secondary rockfall) downslope (e.g. Rapp 1960, Krautblatter and Dikau, 2007), move in a combination of falling, bouncing, rolling or sliding (e.g. Luckman, 2013a, Crosta et al., 2015) and are subsequently deposited on storage landforms (e.g. talus cone). Depending on their magnitude, they pose a potential natural hazard (e.g. Dorren, 2003) and can cause damage to human

https://doi.org/10.5194/nhess-2020-322
Preprint. Discussion started: 6 October 2020
© Author(s) 2020. CC BY 4.0 License.

lives and local infrastructure facilities (e.g. Pfeiffer and Bowen, 1989, Dorren, 2003, Ravanel et al., 2010, Volkwein et al., 2011, Frattini et al., 2012, Heiser et al., 2017).

The occurrence and magnitude of rockfall depend on the preconditioning and the preparatory factors (e.g. Meißl, 1998, Dorren, 2003, Dietze et al., 2017a) as well as on triggering events. The preconditioning and preparatory factors are mainly: lithology, topography of the slope (aspect, steepness, altitude), vegetation (e.g. Meißl, 1998, Jaboyedoff and Derron, 2005), rainfall and weathering, frequency of freeze/thaw cycles, sun exposure and root growth (e.g. Meißl, 1998, Jaboyedoff and Derron, 2005, Krautblatter and Dikau, 2007, Frattini et al., 2012, Crosta et al., 2015).

Due to the economic and societal importance, especially in the context of global change, many studies exist about rockfall processes, focusing on the modelling of runout trajectories and the prediction of rockfall events (e.g. Kirkby and Statham, 1975, Meißl, 1998, Agliardi and Crosta, 2003, Dorren 2003, Copons et al., 2009, Jaboyedoff and Labiouse, 2011, Frattini et al., 2012, Nappi et al., 2013, Wichmann, 2017, Volkwein et al., 2018, Caviezel et al., 2019), as well as on the measurement of rockfall activity by seismic monitoring (e.g. Vilajosana et al., 2008, Hibert et al., 2011, Farin et al., 2015, Dietze et al., 2017a, Dietze et al., 2017b, Durand et al., 2018, Feng et al., 2019). Most of these studies use LiDAR (light detection and ranging), techniques such as airborne laser scanning (ALS) as well as terrestrial laser scanning (TLS) to improve the understanding of this geomorphic process (e.g. Jaboyedoff et al., 2007, Abellán et al., 2011, Haas et al., 2012, Heckmann et al., 2012, Royán et al., 2014, Strunden et al., 2015, Sala et al., 2019). In recent times Structure-from-Motion (SfM) is also increasingly used for such kind of studies (e.g. Kromer et al. 2019, Vanneschi et al., 2019, Guerin et al., 2020).

In the context of hazard assessment, but also for geomorphological models, not only the transported volumes, but also the analysis of the maximum runout distance of blocks plays an important role especially in populated mountain regions (e.g. Jaboyedoff and Labiouse, 2011, Volkwein et al., 2011, Lambert et al., 2013, Caviezel et al., 2019). Factors influencing the runout distance and the track of blocks include properties of the blocks itself (size and shape) and the characteristics of the topographical conditions of the talus cone, including e.g. roughness (e.g. Meißl, 1998, Frattini et al., 2012). The size and shape of the blocks are considered to be a controlling factor for the travel distance (e.g. Pfeiffer and Bowen, 1989, Leine et al., 2014), as they influence the inertia moment of a block and as a consequence its runout trajectory (e.g. Frattini et al., 2012).

The influence of block shape, block size and slope topography on the runout distance was investigated only by a rare number of studies (Azzoni and de Freitas, 1995, Haas et al., 2012, Fityus et al., 2013) and mainly in case studies or tests under laboratory conditions (Okura et al., 2000, Glover et al., 2015, Wang et al., 2018). Haas et al. (2012) already stated in their case study that the influence of the lithology on block shape and block size must be investigated with a broader view. This could be done e.g. in areas with different lithological settings, as the size and shape of rock fragments are determined by their lithological properties, among other influencing factors (Haas et al., 2012, Fityus et al., 2013). Some studies described the deposition of boulders on the talus cone as gravitational sorting, where larger blocks are deposited in the proximal part of the talus slope and smaller blocks at the upper part (e.g. Statham, 1973, Whitehouse and McSaveney, 1983, Kotarba and Strömquist, 1984, White, 1981, Jomelli and Francou, 2000, Sanders et al., 2009, Messenzehl and Dikau, 2017, Popescu et al., 2017, Kenner, 2019). The sorting of the blocks on the slope is a key factor for the roughness component of talus slopes and

https://doi.org/10.5194/nhess-2020-322
Preprint. Discussion started: 6 October 2020
© Author(s) 2020. CC BY 4.0 License.

Natural Hazards and Earth System Sciences Discussions

thus on the runout length of following rockfall events (Hungr and Evans, 1988), indicating a potential feedback loop in the formation of talus landforms.

The aim of this study is to carry out a comparative investigation of the morphometric properties and runout distances of rockfall fragments in mountain regions within different lithological settings. We selected four sites with different lithological conditions and different rockfall activity. For the two study sites PF and ZBT the blocks cannot be assigned to one single rockfall. Whereas the blocks of the other two study sites GA and DTS can be assigned to a rockfall event. Due to lithological differences of the cliffs, we expected different statistical distributions of block sizes and block shapes on the talus slopes. The study is conducted using high-resolution digital terrain models (DTMs) created from TLS surveys. Based on the research of Haas et al. (2012), we determined different block properties (size and shape) and analysed them in the context of runout distances and talus morphology.

2. Study Sites

Four areas in high mountainous regions were selected for this investigation. Three of these areas are situated in the Alps (Fig. 1), one area is located on the island of La Réunion (Fig. 2). The areas differ mainly with regard to the lithological conditions. All areas are characterized by a recent rockfall activity and a clearly distinguishable rock face with an associated scree slope. A further criterion for the selection of the area was that both the rock faces and the talus cones were clearly and completely visible to ensure a complete and dense LiDAR acquisition.

https://doi.org/10.5194/nhess-2020-322
Preprint. Discussion started: 6 October 2020
© Author(s) 2020. CC BY 4.0 License.

Natural Hazards and Earth System Sciences
Discussions
Open Access
EGU

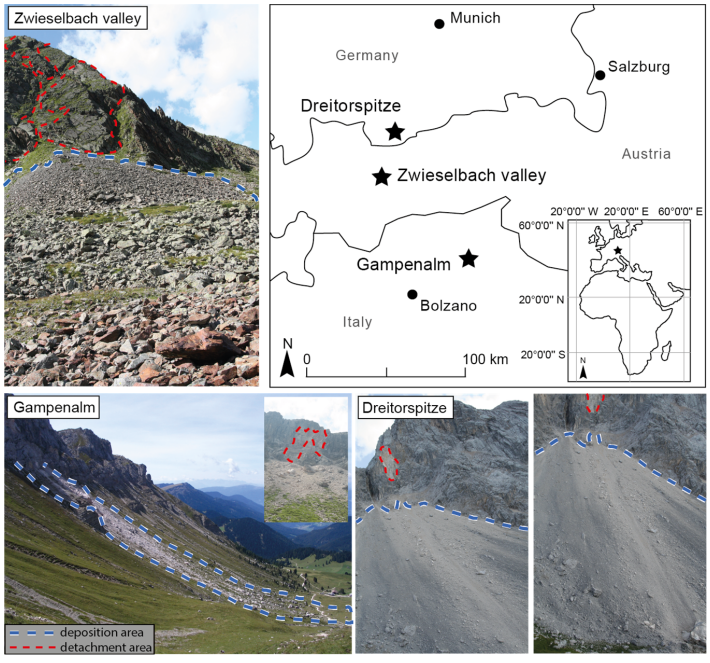

Figure 1. Geographical location of the three study areas located in the European Alps (Dreitorspitze, Zwieselbach valley and Gampenalm). The stars locate the location of the study sites. The red dotted lines limit the detachment areas of the rockfall events. The blue and white dotted lines represent the deposition area. (Source of the overview base map: Esri, HERE, Garmin, OpenStreetMap, contributors and the GIS user community).

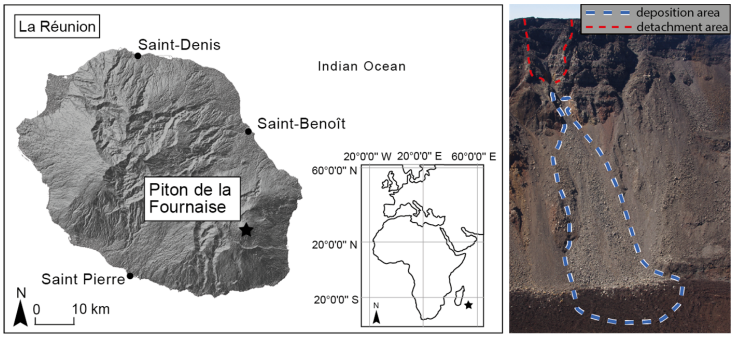

Figure 2. Geographical location of the study area Piton de la Fournaise on the La Réunion island. The star locates the location of the study site. The red dotted lines limit the detachment areas of the rockfall events. The blue and white dotted lines represent the deposition area. (Source of the overview base map: Esri, HERE, Garmin, OpenStreetMap, contributors and the GIS user community).

https://doi.org/10.5194/nhess-2020-322
Preprint. Discussion started: 6 October 2020
© Author(s) 2020. CC BY 4.0 License.

95 The areas Gampenalm (GA) and Dreitorspitze (DTS) are located in the southern and the northern Alps and are made up of sedimentary rocks specifically of different limestone formations (Table 1). The GA area is located in the Dolomites and is dominated by the thick banked/untreated Rosengarten Dolomite (c.f. Haas et al., 2012), the DTS is dominated by the thick banked/untreated Wetterstein limestone. In both areas, major rockfall events occurred in recent years.

The Zwieselbach valley (ZBT) in the Stubaier Alps is located in the area of the crystalline Central Alps and is characterized 100 by slated gneiss and metamorphic granites. Major rockfall events during the last years are not known, but the deposits on the talus cone show indicate rockfall activity.

Table 1. Morphological and lithological characteristics of all investigated talus slopes.

Study Area	PF	ZBT	GA	DTS
Altitude	2632 m a.s.l.	2278 m a.s.l.	2450 m a.s.l.	2682 m a.s.l.
Lithology	Basalt	Gneisses, glimmers, metamorphic granits	Triassic dolomites, limestone, psephite	Triassic limestone, dolomite
Mean slope inclination				
talus cone	36°	29°	32°	32°
cliff	55°	50°	59°	66°
Length of				
talus cone	250 m	55 m	250 m	300 m
cliff	150 m	60 m	150 m	100 m
Mean annual precipitation	3000–4250 mm $year^{-1}$	1000 mm $year^{-1}$	862.2 mm $year^{-1}$	1500 mm $year^{-1}$
Mean annual temperature	13.8° C	0.9° C	7.8° C	6.7° C

105 The test site Piton de la Fournaise (PF, Dolomieu crater) on La Réunion is the only area outside the Alps and is located in the Indian Ocean, east of Africa, but politically it belongs to France as an overseas department. PF is one of the most active volcanoes in the world (e.g. Peltier et al., 2009a) with an average of one eruption every 5.3 months since 2014 (e.g. Derrien et al., 2018). Due to a summit collapse during an eruption in 2007 (e.g. Peltier et al., 2009b) a 340 m deep caldera was formed (e.g. Staudacher et al., 2016) on an area of 1100 x 800 m (e.g. Urai et al., 2007). On this volcano, the composition of the lava 110 is mainly bimodal with a combination of aphyric basalts and olivine rich basalts (e.g. Peltier et al., 2009a, Lénat et al., 2012). Due to the high tectonic stress (e.g. Merle et al., 2010, Staudacher et al., 2016), the high volcanic activity that generate

https://doi.org/10.5194/nhess-2020-322
Preprint. Discussion started: 6 October 2020
© Author(s) 2020. CC BY 4.0 License.

deformation and seismic activity (e.g. Sens-Schönfelder et al., 2014, Peltier et al., 2018) and the layering of different lava flows, the rim is very unstable and thus prone to high rockfall dynamics. This area certainly differs most clearly from all other studied areas. Besides the volcanic rocks, both the cliff and the talus cones are very young landforms, as the geomorphic forming started right after the emergence of the caldera in 2007. Further differences are the high deformation and seismic activity and the extremely high precipitation. Both factors certainly play an important role for the rockfall activity (daily rockfall activity), but should not have any influence on the runout lengths of single blocks, so that for the present investigations primarily the differences in lithology and in the case of PF the age have to be considered.

3. Materials and methods

3.1 Data acquisition and processing (TLS)

The data of all study sites have been acquired with a terrestrial 3D long range laser scanner. Two systems were used: the Riegl LMS-Z420i and the Riegl VZ-4000. Both scanner work on the same principle (time of flight), but due to laser configurations, the scanning distance of the VZ-4000 is four times longer (4000 m compared to 1000 m). Both systems provide colour information due to integrated camera systems in order to colorize the point clouds. All important technical information of both devices is listed in Table 2.

Due to the special conditions of the Dolomieu crater (longer distance between scanner and target, poor reflectance of the volcanic material) we used the VZ-4000 for this study site, all other test sites were surveyed using the LMS-Z420i. To minimize shadowing effects, several scan positions were necessary at each site, which had to be referenced using manual adjustment and ICP algorithms (Table 3), which are implemented in the software RiScan Pro (v2.2.1 www.riegl.com).

Table 2. Technical data of the two terrestrial laser scanning systems Riegl LMS-Z420i and VZ-4000 (RIEGL Laser Measurement Systems GmbH, 2010, RIEGL Laser Measurement Systems GmbH, 2020). The values of the VZ-4000 refer to measurements at a rate of 30 kHz.

	LMS-Z420i	VZ-4000
Max. measurement range	1000 m	4000 m
Measurement rate	8000 pts./sec.	23000 pts./sec.
Accuracy	10 mm	15 mm
Precision	4–8 mm	10 mm
Laser wavelength	Near infrared	Near infrared
Laser beam divergence	0.25 mrad	0.15 mrad

After the referencing, the data were exported as ASCII files containing x, y, and z coordinates as well as RGB values for further analysis in SAGA GIS/LIS (Conrad et al., 2015; Laser Information System LIS: www.laserdata.at). Based on the point

https://doi.org/10.5194/nhess-2020-322
Preprint. Discussion started: 6 October 2020
© Author(s) 2020. CC BY 4.0 License.

Natural Hazards and Earth System Sciences
Discussions

clouds we created digital terrain models (DTMs) for all test sites with a raster resolution of 0.75 m using the lowest z value. Table 3 provides information about each study site including the vertical and horizontal scan resolution, the referencing precision, number of points in the raw data set and the point density (points/m²).

Table 3. Information about the TLS surveys for each study area.

	TLS system	Scan resolution	Referencing precision	Number of points raw data set	Point density (pts/m²)
PF	VZ-4000	0.02°	0.007–0.013 m	> 60x10^6 points	55 pts/m²
ZBT	LMS-Z420i	0.05°–0.1°	0.018–0.060 m	1.5x10^6 points	50 pts/m²
GA	LMS-Z420i	0.05°–0.1°	0.012–0.058 m	8x10^6 points	54 pts/m²
DTS	LMS-Z420i	0.05°–0.2°	0.015–0.065 m	3x106 points	54 pts/m²

3.2 Determination of block size, block shape and runout length

According to the workflow of Haas et al. (2012) we measured the dimensions of the three axes (a, b and c) of single boulders for every study area (PF: n=255, GA: n=618, ZBT: n=65, DTS: n=182) from the upper to the lower parts of the talus cones. Based on the coloured LiDAR point clouds every block larger than c. 0.5 m (longest axis) was manually measured in the software RiScan Pro. Figure 3 shows an idealized sketch of a boulder with the three measured axes.

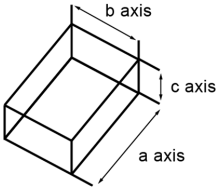

Figure 3. Schematic illustration of a block with the three measured dimensions of the axes a, b and c.

By using the measured three axes, the volume (Eq. 1) and the block shape (axial ratio) (Eq. 2) can be approximated. We followed the work of Haas et al. (2012), which used the formula of Valeton (1955) as an indicator of the block shape, where values of 1 means more or less a round shape and values of >>1 more or less an elongated or platy shape.

$$Block\ volume = Axis\ a * Axis\ b * Axis\ c \quad (1)$$

$$Axial\ ratio = Axis\ a / Axis\ b\ / Axis\ c \quad (2)$$

https://doi.org/10.5194/nhess-2020-322
Preprint. Discussion started: 6 October 2020
© Author(s) 2020. CC BY 4.0 License.

Natural Hazards and Earth System Sciences Discussions

For the calculation, the parameter of the axis b must be set to 1 (cf. Valeton, 1955).

The Euclidean distance of each measured boulder to the detachment zone was determined to obtain the runout length (DTS, GA). Since the exact detachment zone could not be determined at PF and ZBT, we measured the Euclidean distance from the beginning of the transition between cliff and talus cone to each boulder instead. To compare the runout distances between the study areas, we normalized the runout lengths for each talus cone to the interval [0,1].

3.3 Morphometric slope properties

Based on the high-resolution DTMs of the study sites we performed a spatial analysis of the talus cones including all morphometric properties with a presumed influence on the deposition (e.g. Wang and Lee, 2010, Frattini et al., 2012, Crosta et al., 2015) and runout distances of rock fall boulders (e.g. Glover et al., 2015): slope inclination, surface roughness (debris texture) and profile curvature. The slope inclinations were derived based on the DTMs according to Zevenbergen and Thorne (1987). The surface roughness was derived after the approach of Frankel and Dolan (2007). They defined the surface roughness as the standard deviation of slope (SDS),

$$SDS = \left[\frac{1}{N^2} \sum_{i=1}^{N^2} (m_i - \bar{m})^2\right]^{0.5} \quad (3)$$

where N is the width of the moving windows (number of cells), m_i is the slope of the i–th cell and $\bar{m}$ the mean slope within the moving window (Eq. 3; Frankel and Dolan, 2007, Berti et al., 2013). We set N to 9 (a 3x3 cell neighbourhood) corresponding to an area of 5.1 m². This results in a spatial distributed roughness map for all talus cones (Grohmann et al., 2010) where the roughness of the slope can also serve as a proxy for the particle size distribution on the talus cone.

Additionally, we created three longitudinal swath profiles (width=10 m) from the highest part of the cone to the distal boundary in order to characterize slope morphology of all four test sites (e.g. segmentation indicated by changes in slope inclination, profile concavity etc, cf. Hergarten et al., 2014) and we applied a kernel density estimation (cf. Cox, 2007) to compare the distributions of slope inclination between rock faces and talus cones, and between the study sites.

4. Results and Discussion

4.1 Morphometric analyses

4.1.1 Block volumes and block shapes

Figure 4 shows the distributions of sizes and shapes of the investigated blocks with the longest axis greater than 0.5 m for the four investigated talus cones. With regard to the block volumes, the four investigated sites differ, in some cases very

https://doi.org/10.5194/nhess-2020-322
Preprint. Discussion started: 6 October 2020
© Author(s) 2020. CC BY 4.0 License.

Natural Hazards and Earth System Sciences
Discussions

significantly. The smallest block sizes (median) can be found in the area ZBT (0.08 m³), the largest block sizes in the area DTS (13.16 m³). The median is below 4 m^3 in the three areas PF (3.38 m³), ZBT (0.08 m³) and GA (1.63 m³). The data dispersion also shows a very homogeneous distribution and only small maximum values in PF and ZBT, whereas in GA and DTS a very large dispersion and high maximum values (GA: 2028.72 m³, DTS: 5784.27 m³) are obvious. This indicates that a correlation between the lithological conditions and the block sizes involved in rockfall processes can be assumed, as the largest blocks are mainly found in areas with banked limestones. This is well visible in the Wetterstein limestone and to a lesser degree in the Dolomite area. The extremely small block sizes are particularly striking in the area of metamorphic rocks (ZBT). This can be explained by the rather slated and thus platy rock structure of the gneisses and by the long tectonic history of these rocks.

In contrast to the block sizes, the block shapes (Fig. 4) in all four areas show a high dispersion between round and rather elongated blocks. The most elongated blocks can be found in the ZBT (median = 2.63) area, which again can be explained by the slated structure of the gneisses. The limestones of the areas GA (median = 2.33) and DTS (median = 2.40) are very similar in both the median block shape and the dispersion of the data. The lowest values and therefore the most round shaped blocks can be found in the area PF (median = 1.73) with its volcanic rocks. Whether this is due to lithology or to tectonic stresses caused by the high seismic activity and the resulting eruptive fissures cannot be finally clarified with the data of this study.

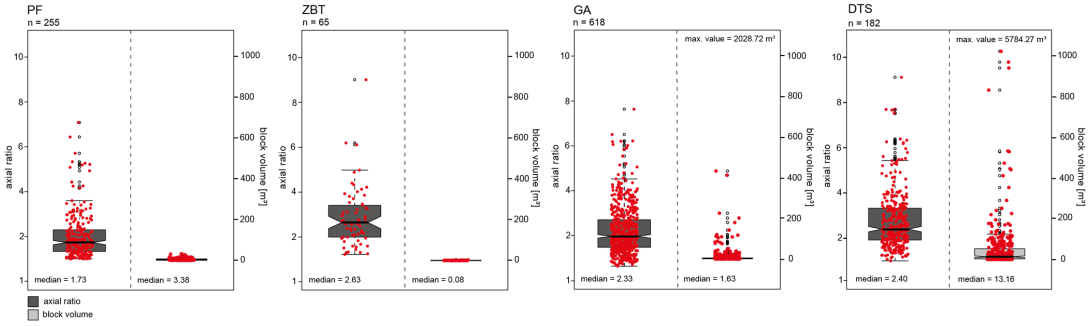

Figure 4. Boxplots of volume and shapes of the measured blocks. The red coloured points correspond to each measured block. The thick black lines within the boxes show the median bounded by the 1st quartile (25th percentile) and the 3rd quartile (75th percentile). The boxes show the interquartile range (IQR). The whiskers of the boxplots mark the minima and maxima of the data. The circles represent data which exceed the 1.5fold IQR.

With regard to the block shapes and block size distributions in the areas, however, it can be concluded that the investigated areas show sufficient differences in both block sizes and shapes, and that this is a consequence of the lithological setting. This allows for a more detailed investigation of the relationships between block shape, block size and runout distance.

https://doi.org/10.5194/nhess-2020-322
Preprint. Discussion started: 6 October 2020
© Author(s) 2020. CC BY 4.0 License.

Natural Hazards and Earth System Sciences
Discussions

4.1.2 Talus cone characteristics

In addition to the block shape and block size, the topography of the talus cones also plays an important role and has to be considered for a runout analysis. Thus, we analysed the following form parameters: slope inclination, curvature/slope profiles and roughness (Fig. 5).

The average slope inclination of the talus cones lies between 28° and 36° and thus within the range for such landforms (e.g. Pérez, 1989, Pérez, 1998, Francou and Manté, 1990, Jomelli and Francou, 2000, Sanders et al., 2009, Luckman, 2013b, Popescu et al., 2017, Volkwein et al., 2018). This can provide an indication of the dependence between rock material and slope inclination of gravel or blocky material and thus supports the findings of other studies.

Kenner et al., (2019) reported in their study (amphibolite sediments) slope angles of 35° and Messenzehl and Dikau (2017) described in their survey (metamorphic rocks) slope angles of 34–36° and 33–34°. The lowest value with 28.9° can be found on ZBT, the highest value on PF with 36.0°. The talus cones DTS and GA show quite similar values (DTS: 31.9°, GA: 31.6°). According to Gerber (1974), the slope inclination is defined by the shape and roughness of the deposited blocks and lies between 18°–43°. In his study he measured slope inclination of 33° for Gneisses and metamorphic granites (ZBT) and 32° for limestone formations (GA, DTS) (Gerber, 1974). Serrano et al., (2019) described in their study slope inclination for limestone formations between 32–36°. Knoblich (1975) gives values of 28°–43°. Yamamoto et al., (2005) conclude that basaltic material cannot be deposited on slopes of more than 33°. The relatively higher average slope inclination at the PF is also interesting. Here, rock surface conditions could also play an important role, since volcanic rocks in particular are characterized by a high micro-roughness of the rock surface and surface friction can govern the natural slope angle of debris material. This is supported by the distributions of the slope inclinations (c.f. Fig. 5D), where the data scatter is lowest in the PF area. Here the distribution is very peaked and differs clearly from the distributions of the other three areas. The shape of the slope profiles (Fig. 5A) also points in a similar direction. The talus cone of PF follows a straight line over the entire length of the slope, whereas the other cones show a slight convexity in the upper and middle slope and a basal concavity at the end of the slope, which is in good agreement with the works of Kotarba and Strömquist (1984), Luckman (2013b), and Popescu et al. (2017). Nevertheless, it is very likely that the talus cone of the PF represents a pure talus cone and is reshaped since then by persistent rockfalls, whereas the talus cones of the other areas represent much older forms where different types of geomorphic processes occur.

The derived roughness shows a clear difference between the study sites (Fig. 5C, 6A). The roughness in PF seems to be continuously increasing in the downslope direction (with the lowest roughness at the upper slope and the highest roughness at the end). On the other talus cones it is noticeable that the highest roughness can be found at the upper slope (somewhat less pronounced in ZBT), then fall off and rise again towards the end of the slope. Roughness can be seen as a factor of the runout length. As seen in Fig. 6A and 7B it can be assumed that for smaller particles roughness on the slope is more decisive than for larger particles that do not get stopped by coarser material. The very straight line of the slope with a high mean slope inclination (PF) compared to the other areas play an important role. Here large blocks seem to overcome almost the full length of the slope, while in the other areas large blocks seem to stop in the upper parts as well as in the lowest parts. The spatial distribution

https://doi.org/10.5194/nhess-2020-322
Preprint. Discussion started: 6 October 2020
© Author(s) 2020. CC BY 4.0 License.

Natural Hazards and Earth System Sciences
Discussions

of the roughness points in the same direction (Fig. 6A). Especially at the PF, where the highest roughness can be found at the lower end of the slope. The largest spatial dispersion of the roughness can be found at GA (median = 6.92), where large blocks and thus high roughness seems to be distributed over the whole talus cone. To a slightly lesser extent this also applies to DTS (median = 4.86). These high roughness values can influence the deposition of rock fragments as they act like a natural obstacle and can influence the trajectories of future rockfall events. This deposition and accumulation of material can be explained by the straight and steep slope with a minor basal concavity. At the same time, the highest roughness values can be found at GA and DTS, the lowest at ZBT (median = 4.75) and PF (median = 4.67), which can be associated with the different block volume distribution. The analyses show that surface complexity and roughness are not the only parameters which are important for gravitational sorting to take effect.

https://doi.org/10.5194/nhess-2020-322
Preprint. Discussion started: 6 October 2020
© Author(s) 2020. CC BY 4.0 License.

Natural Hazards and Earth System Sciences
Discussions

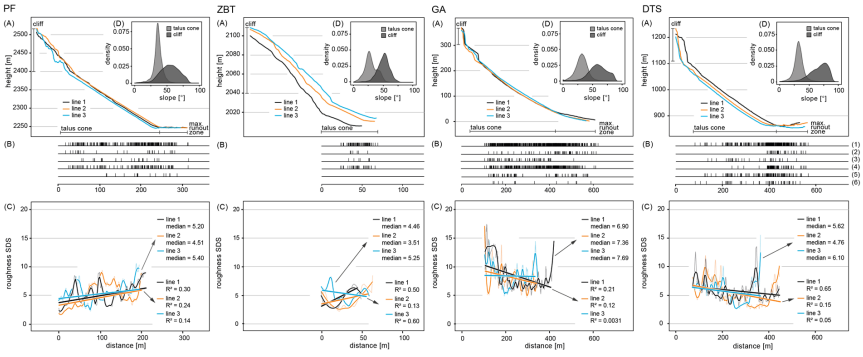

Figure 5. Three swath longitudinal profiles from the cliff to the maximum runout distance (A). Statistical distribution of all measured blocks regarding their shapes and volumes on the talus cone. Every single line represents a measured block and thus the deposition on the slope can be illustrated. For this purpose, we have presented all blocks (1), the most (2) and least (3) spheroidal blocks and we have classified the block volume according to 10 m³ (4), 10² m³ (5) and 10³ m³ (6) (B). Calculated roughness values with the approach of standard deviation of slope (SDS) for the three longitudinal profiles. The thick lines represent the moving average and the thin lines represent the original data. Additionally, calculated regression line and R^2 of each longitudinal profile with roughness values (C). Kernel density estimation of slope inclination distinguished according to the cliff and the talus cone (D).

https://doi.org/10.5194/nhess-2020-322
Preprint. Discussion started: 6 October 2020
© Author(s) 2020. CC BY 4.0 License.

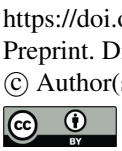

Natural Hazards and Earth System Sciences
Discussions
Open Access
EGU

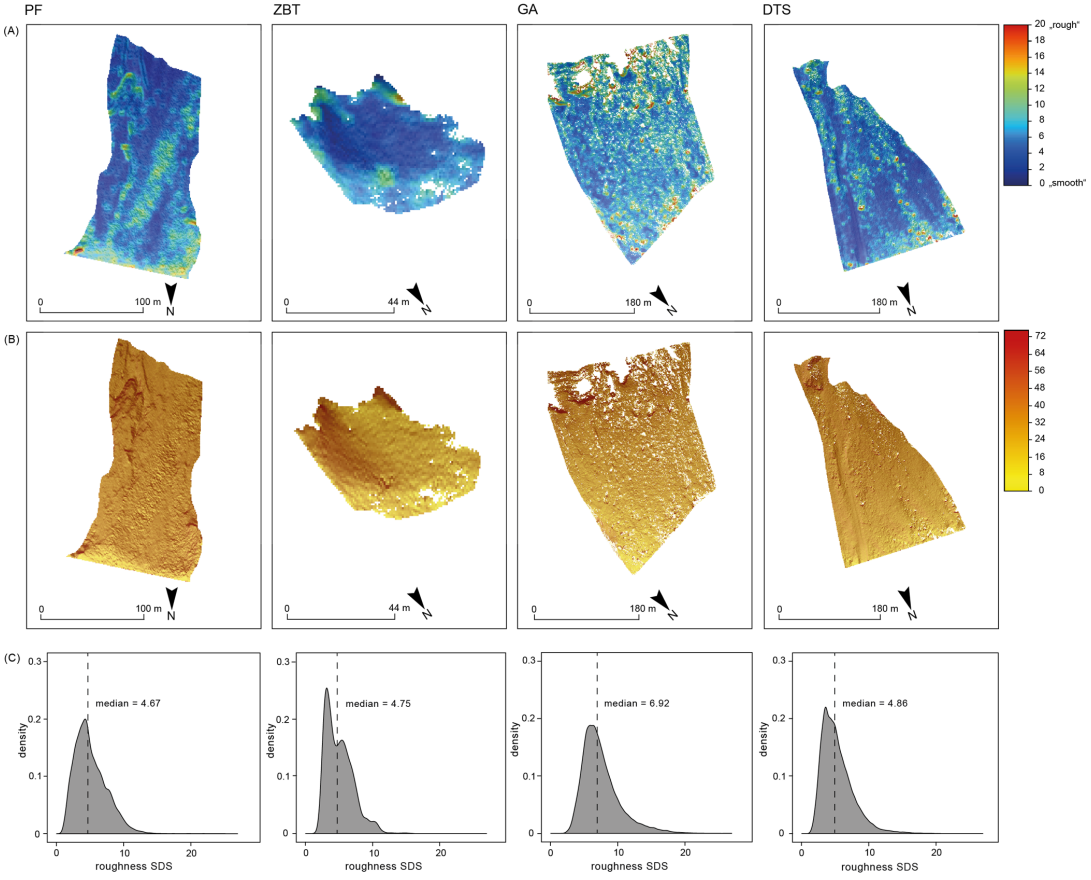

Figure 6. Maps showing the spatial roughness values for the talus cone of each study area. Red areas indicate a rough surface and blue areas indicate a less rough surface (A). Maps of slope inclination for the talus cone (B). Kernel density estimation of roughness values for the talus cone with marked median values (black dotted line) (C).

4.2 Relationship between block size, block shape and runout length

In order to analyse the relationship of block volume, block shape and runout length, we calculated a Spearman rank correlation (Table 4). The results show only weak correlations between block volume and runout distance as well as weak correlations between runout length and block shape for the four test sites, which indicate no monocausal relationship.

These results are in contrast to other studies. Jomelli and Francou (2000) state that longitudinal sorting of talus cones shows an increase of block sizes downslope. In their study, Popescu et al. (2017) conclude that there is a gradual increase of boulder

https://doi.org/10.5194/nhess-2020-322
Preprint. Discussion started: 6 October 2020
© Author(s) 2020. CC BY 4.0 License.

Natural Hazards and Earth System Sciences Discussions

size towards the slope base. Serrano et al. (2019) showed that the distal part of a slope is defined by the accumulation of large blocks. In contrast to these studies Caine (1967) found a decrease of blocks sizes with distance downslope, but his results are statistically insignificant. Messenzehl and Dikau (2017) found, that there is a distinct downslope increase in block size and sphericity, which indicates a combination of these block characteristics govern the runout length.

285

Table 4. Analysis of the relationship of block volume, axial ratio against runout length by means of Spearman rank correlation for each study site.

	PF	ZBT	GA	DTS
Block volume rho	0.15	0.33	-0.04	-0.29
Block volume p-Value	0.02	0.007111	0.39	<<0.001
Axial ratio rho	0.06	0.27	-0.35	-0.42
Axial ratio p-Value	0.36	0.03	<<0.001	<<0.001

Thus and in accordance to Haas et al. (2012) we plotted the relative distance against log10 block volume to show the
290 relationship for every single talus cone in more detail (Fig. 7). We combined this analysis with the axial ratio of the boulders. Figure 7A shows boxplots with six different quantile classes (<q10, q10–q25, q25–q50, q50–q75, q75–q90, >q90), which correspond to the 10, 25, 50, 75 und 90 % quantiles of the log10 block volume and log10 axial ratio. To analyse the relationship of the parameters in more detail, we highlighted the 10 % (low axial ratio, most spheroidal blocks, small volume) and the 90 % (high axial ratio, least spheroidal blocks, large volume) quantile classes, which are visualized with different symbols and
295 colours (Fig. 7B).

Figure 7 shows that there are some significant differences between the individual areas and that the areas can be divided into two groups with regard to runout length, block size and block shape. The first group consists of the areas GA and DTS, the second group consists of PF and ZBT. Furthermore, GA and DTS primarily include blocks of one rockfall event, while the blocks of PF and ZBT cannot be assigned to one rockfall event.

300 GA and DTS clearly show that the size of the blocks obviously does not play a major role for the runout length on the talus cones (the median values do not show a significant trend), but the dispersion of the runout distances clearly increases with increasing block size. This is visible in both areas, but is more pronounced at DTS. But it is also visible that blocks with larger volumes are also having smaller runout distances (Fig. 7). The scatterplots show, in accordance with Fig. 7A, that the block size scatters strongly over the entire talus cone. The block size can therefore not be used as an explanation for the runout
305 distance alone, which is in agreement with the Spearman rank correlation.

The situation is different regarding the block shapes in the two areas. Here it is clearly visible that with increase in axial ratio, the runout distance decreases. This is also quite consistent with the results of the Spearman-Rank correlation, because in these two areas a slight correlation between axial ratio and range can be stated (GA: r = –0.35, DTS: r = –0.42). However, this is

https://doi.org/10.5194/nhess-2020-322
Preprint. Discussion started: 6 October 2020
© Author(s) 2020. CC BY 4.0 License.

Natural Hazards and Earth System Sciences
Discussions

also visible in Fig. 7B, which shows the roundest and longest blocks combined with the ranges: round blocks (<q10) reach larger distances than elongated blocks (>q90) (e.g. Pérez 1998). This can be seen in both areas from a relative distance of about 0.7 on the talus cone. We observed that the parameter axial ratio acts like a moderating parameter with regard to the deposition of blocks. Pérez (1998) and Messenzehl and Dikau (2017) also conclude in their study that rounder blocks are deposited predominantly at the talus toe. As already shown by Glover et al. (2015) in their rockfall simulation, uniformly shaped blocks followed by elongated blocks achieve the largest ranges. This is due to the fact, that boulders with a low axial ratio roll over any axis and do not lose momentum. Platy blocks on the other hand reach the shortest runout distances (Glover et al., 2015). It is particularly noticeable, however, that in the DTS area all very round blocks (<q10) achieve very high ranges and are not found at all in the shorter distances. This is different in the GA area. Here the majority of the round blocks can be found at the end of the slope, but also at the upper slope. This could be due to the fact that during the rockfall event the blocks collided with each other (maybe split into smaller blocks), resulting in the different block shapes being deposited in both the lower and the upper area of the talus cone (Ruiz-Carulla and Corominas, 2020). However, this could not be fully clarified in the context of this analysis.

In the areas ZBT and PF the situation is clearly different, here the block sizes seem to have a recognizable influence on the runout length. Although the dispersion of the data and the Spearman-Rank correlation show that this correlation is not significant (Table 5, PF: r = 0.15, p-value = 0.02, ZBT: r = 0.33, p-value = 0.007111), large blocks above a certain size are no longer found in the short runout lengths. However, Fig. 7 also shows that for PF, smaller and larger blocks are deposited in all areas of the slope. At the same time, unlike GA and DTS, the block shape does not seem to play a role for the runout distance, which is also indicated by the Spearman rank correlation, PF: r = 0.06, ZBT: r = 0.27. Round and elongated blocks are actually found over the entire talus cone without any visible clustering (Fig. 7).

https://doi.org/10.5194/nhess-2020-322
Preprint. Discussion started: 6 October 2020
© Author(s) 2020. CC BY 4.0 License.

Natural Hazards and Earth System Sciences
Discussions
Open Access
EGU

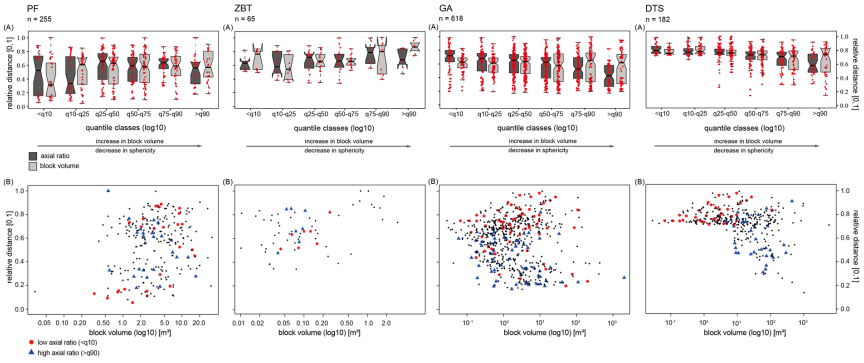

Figure 7. Boxplots of relative distance versus log10 block volume and log10 block shapes of the measured rocks for each study site (A). The red coloured points correspond to each measured individual block. The thick black lines within the boxes show the median bounded by the 1st quartile (25th percentile) and the 3rd quartile (75th percentile). The boxes show the interquartile range (IQR). The whiskers of the boxplots mark the minima and maxima of the data. The circles represent data that exceed the 1.5fold IQR (A). Scatterplot of relative distance versus log10 block volume for all study sites. Blocks with a low axial ratio (<q10) and a high axial ratio (>q90) are highlighted with different colours and symbols (B).

https://doi.org/10.5194/nhess-2020-322
Preprint. Discussion started: 6 October 2020
© Author(s) 2020. CC BY 4.0 License.

5. Conclusion

In this study a comparative analysis of morphometric properties and run out lengths of rockfall fragments in mountainous regions within different lithological conditions was conducted.

Our study shows a recognizable correlation between block size and block shape depending on the lithology, which results in larger blocks with higher sphericity in areas with thick banked/untreated limestones (GA, DTS), smaller and platy/elongated blocks in areas with slated gneiss and metamorphic granites (ZBT) and smaller and more spherical blocks in basaltic lava material (PF).

Our analyses reveal a complex relation between block size and block shape with respect to the travel distance of deposited blocks with divergences between different lithological settings. Compared to other studies (Whitehouse and McSaveney, 1983, Jomelli and Francou, 2000, Sanders et al., 2009, Luckman, 2013a, Messenzehl and Dikau, 2017, Popescu et al., 2017) and with respect to our results we can neither confirm nor reject the theory of gravitational sorting (Fig. 7), as we cannot confirm, that blocks with smaller volumes have decreasing runout distances. In fact, some of the results provide a negative relationship of block volume and runout distance, which results in increasing block volume with decreasing runout distances (Fig. 7).

As the block size does not seem to be the only control variable, the axial ratio of boulders seems to influence the deposition of rock fragments on the talus cone such that blocks with increasing sphericity have increasing runout distances (Pérez, 1998, Glover et al., 2015, Messenzehl and Dikau, 2017, Volkwein et al., 2018). This is due to the fact that boulders with a low axial ratio (high sphericity) roll over any axis and do not lose momentum. In our study, we could show that spherical shaped boulders are deposited not only in the distal part of the talus cone but also in the proximal area (Fig. 7). For the study area GA and DTS we observed that the parameter axial ratio acts like a moderating parameter with regard to the deposition of blocks. Accordingly, most spheroidal blocks have increasing runout distances and least spheroidal blocks have decreasing runout distances. In case of PF and ZBT we cannot confirm the hypothesis of a moderating role of the axial ratio. Whether this is due to the different lithological setting or the fact that GA as well as in DTS primarily included blocks of one rockfall event, while the blocks in PF and ZBT represent several individual and presumably temporally unrelated block falls, cannot finally be clarified and has to be tested in the future.

Regarding the talus cone characteristics, PF has the highest slope inclinations, followed by GA, DTS and ZBT with the lowest values (Fig. 5D, 6B). When considering the talus cone characteristics, it must be taken into account that PF represents a pure slope, which is reshaped by persistent rockfalls. The other areas are older slopes that are influenced by different types of geomorphic processes besides rockfalls. Apart from the slope inclination, differences between the longitudinal profiles (straight slope of the PF and more slight convexity in the upper and middle slope and a basal concavity at the end of the slope of the other areas) should be mentioned (Fig. 5A). The roughness values can be associated with the different block volume distribution and can be seen as a factor of the runout length. The highest roughness values as well as block volumes are found

https://doi.org/10.5194/nhess-2020-322
Preprint. Discussion started: 6 October 2020
© Author(s) 2020. CC BY 4.0 License.

Natural Hazards and Earth System Sciences Discussions

in the GA area and in DTS (Fig. 5C, 6A). In contrast, the smallest values have PF and ZBT (Fig. 5C, 6A). Roughness influences the deposition of blocks and their trajectories as it acts like a natural obstacle.

As the sample of different source rocks is quite small (four test sites), this must be seen as an indication of a relationship between lithological conditions and block size/block shape, but should be verified by further studies with larger samples. We are quite sure, that such a study can be done on the base of ALS data or photogrammetric elevation models based on aerial photographs, where point densities are high enough to resolve blocks of a certain size, which are nowadays available for the whole Alps and mountain ranges worldwide.

Data availability.

The data used in this study are accessible upon request by contacting Kerstin Wegner (KWegner@ku.de).

Author contributions.

KW, FH and TH designed the conceptual idea of the manuscript. KW and FH collected the terrestrial laser scanning data on La Réunion. FH collected the TLS data of DTS, ZBT and GA. TH contributed to statistical analysis of data. VD, NV and PK acquired the dGPS data on La Réunion. NV, PK and AP contributed to fieldwork on La Réunion. AM contributed to the financial support of the travel costs to La Réunion. MB contributed to the acquisition of the terrestrial laser scanner. KW wrote the manuscript with discussions and improvements from all co-authors.

Competing interests.

The authors declare that they have no conflict of interest.

Acknowledgements.

F. Haas kindly provided the photographs used for Fig. 1, 2. The field work on La Réunion was funded by ERC Slidequakes. This is IPGP contribution number TEXT.

References

Abellán, A., Vilaplana, J. M., Calvet, J., García-Sellés, D. and Asensio, E.: Rockfall monitoring by terrestrial laser scanning - case study of the basaltic rock face at Castellfollit de la Roca (Catalonia, Spain), Nat. Hazards Earth Syst. Sci., 11, 829–841, https://doi.org/10.5194/nhess-11-829-2011, 2011.

https://doi.org/10.5194/nhess-2020-322
Preprint. Discussion started: 6 October 2020
© Author(s) 2020. CC BY 4.0 License.

Agliardi, F. and Crosta, G. B.: High resolution three-dimensional numerical modelling of rockfalls, Int. J. Rock Mech. Min., 40, 455–471, https://doi.org/10.1016/S1365-1609(03)00021-2, 2003.

Azzoni, A. and de Freitas, M. H.: Experimentally gained parameters, decisive for rock fall analysis, Rock Mech Rock Eng, 28, 111–124, https://doi.org/10.1007/BF01020064, 1995.

Bennett, G. L., Molnar, P., Eisenbeiss, H. and McArdell, B. W.: Erosional power in the Swiss Alps: Characterization of slope failure in the Illgraben, Earth Surf. Process. Landforms, 37, 1627–1640, https://doi.org/10.1002/esp.3263, 2012.

Berti, M., Corsini, A. and Daehne, A.: Comparative analysis of surface roughness algorithms for the identification of active landslides, Geomorphology, 182, 1–18, https://doi.org/10.1016/j.geomorph.2012.10.022, 2013.

Caine, N.: The texture of talus in Tasmania, J Sediment Res, 37, 796–803, https://doi.org/10.1306/74D717A3-2B21-11D7-8648000102C1865D, 1967.

Caviezel, A., Demmel, S. E., Ringenbach, A., Bühler, Y., Lu, G., Christen, M., Dinneen, C. E., Eberhard, L. A., von Rickenbach, D. and Bartelt, P.: Reconstruction of four-dimensional rockfall trajectories using remote sensing and rock-based accelerometers and gyroscopes, Earth Surf. Dynam., 7, 199–210, https://doi.org/10.5194/esurf-7-199-2019, 2019.

Conrad, O., Bechtel, B., Bock, M., Dietrich, H., Fischer, E., Gerlitz, L., Wehberg, J., Wichmann, V. and Böhner, J.: System for Automated Geoscientific Analyses (SAGA) v. 2.1.4., Geosci. Model Dev., 8, 1991–2007, https://doi.org/10.5194/gmd-8-1991-2015, 2015.

Copons, R., Vilaplana, J. M. and Linares, R.: Rockfall travel distance analysis by using empirical models (Solà d'Andorra la Vella, Central Pyrenees), Nat. Hazards Earth Syst. Sci., 9, 2107–2118, https://doi.org/10.5194/nhess-9-2107-2009, 2009.

Cox, N. J.: Kernel estimation as a basic tool for geomorphological data analysis, Earth Surf. Process. Landforms, 32, 1902–1912, https://doi.org/10.1002/esp.1518, 2007.

Crosta, G. B., Agliardi, F., Frattini, P. and Lari, S.: Key issues in rock fall modeling, hazard and risk assessment for rockfall protection, in: Engineering Geology for Society and Territory, 2, Landslide Processes, edited by: Lollino, G., Giordan, D., Crosta, G., Corominas, J., Azzam, R., Wasowski, J. and Sciarra, N., Springer, International Publishing, Switzerland, 43–58, https://doi.org/10.1007/978-3-319-09057-3_4, 2015.

https://doi.org/10.5194/nhess-2020-322
Preprint. Discussion started: 6 October 2020
© Author(s) 2020. CC BY 4.0 License.

Derrien, A., Villeneuve, N., Peltier, A. and Michon, L.: Multi-temporal airborne structure-from-motion on caldera rim: Hazard, visitor exposure and origins of instabilities at Piton de la Fournaise, Progress in Physical Geography: Earth and Environment, 1–22, https://doi.org/10.1177/0309133318808201, 2018.

Dietze, M., Turowski, J. M., Cook, K.L. and Hovius, N.: Spatiotemporal patterns, triggers and anatomies of seismically detected rockfalls, Earth Surf. Dynam., 5, 757–779, https://doi.org/10.5194/esurf-5-757-2017, 2017a.

Dietze, M., Mohadjer, S., Turowski, J. M., Ehlers, T. A. and Hovius, N.: Seismic monitoring of small alpine rockfalls - validity, precision and limitations, Earth Surf. Dynam., 5, 653–668, https://doi.org/10.5194/esurf-5-653-2017, 2017b.

Dorren, L. K. A.: A review of rockfall mechanics and modelling approaches, Progress in Physical Geography: Earth and Environment, 27, 69–87, https://doi.org/10.1191/0309133303pp359ra, 2003.

Durand, V., Mangeney, A., Haas, F., Jia, X., Peltier, A., Hibert, C., Ferrazzini, V., Kowalski, P., Lauret, F., Brunet, C., Satriano, C., Wegner, K., Delorme, A., Bonilla, F. and Villeneuve, N.: On the link between external forcings and slope instabilities in the Piton de la Fournaise summit crater, Reunion Island, J Geophys Res: Earth Surface, 123, 2422–2442, https://doi.org/10.1029/2017JF004507, 2018.

Feng, L., Pazzi, V., Intrieri, E., Gracchi, T. and Gigli, G.: Rockfall seismic features analysis based on in situ tests: frequency, amplitude, and duration, J. Mt. Sci., 16, 955–970, https://doi.org/10.1007/s11629-018-5286-6, 2019.

Fityus, S. G., Giacomini, A. and Buzzi, O.: The significance of geology for the morphology of potentially unstable rocks, Eng Geol, 162, 43–52, https://doi.org/10.1016/j.enggeo.2013.05.007, 2013.

Francou, B. and Manté, C.: Analysis of the segmentation in the profile of alpine talus slopes, Permafrost Periglac, 1, 53–60, https://doi.org/10.1002/ppp.3430010107, 1990.

Frankel, K. L. and Dolan, J. F.: Characterizing arid region alluvial fan surface roughness with airborne laser swath mapping digital topographic data, J. Geophys. Res., 112, 1–14, https://doi.org/10.1029/2006JF000644, 2007.

Frattini, P., Crosta, G. B. and Agliardi, F.: Rockfall characterization and modeling, in: Landslides, Types, Mechanisms and Modeling, edited by: Clague, J. J. and Stead, D., Cambridge University Press, Cambridge, United Kingdom, 267–281, https://doi.org/10.1017/CBO9780511740367.023, 2012.

https://doi.org/10.5194/nhess-2020-322
Preprint. Discussion started: 6 October 2020
© Author(s) 2020. CC BY 4.0 License.

Gerber, E.: Klassifikation von Schutthalden, Geogr. Helv., 29, 73–82, https://doi.org/10.5194/gh-29-73-1974, 1974.

Glover, J., Bartelt, P., Christen, M. and Gerber, W.: Rockfall-simulation with irregular rock blocks, in: Engineering Geology for Society and Territory, Volume 2, edited by: Lollino, G., Giordan, D., Crosta, G.B., Corominas, J., Azzam, R., Wasowski, J. and Sciarra, N., Springer, International Publishing, Switzerland, 1729–1733, https://doi.org/10.1007/978-3-319-09057-3_306, 2015.

Grohmann, C. H., Smith, M. J. and Riccomini, C.: Multiscale analysis of topographic surface roughness in the Midland Valley, Scotland, IEEE Transactions on Geoscience and Remote Sensing, 49, 4, 1200–1213, 10.1109/TGRS.2010.2053546, 2010.

Guerin, A., Stock, G. M., Radue, M. J., Jaboyedoff, M., Collins, B. D., Matasci, B., Avdievitch, N. and Derron, M.-H.: Quantifying 40 years of rockfall activity in Yosemite Valley with historical Structure-from-Motion photogrammetry and terrestrial laser scanning, Geomorphology, 356, 1–18, https://doi.org/10.1016/j.geomorph.2020.107069, 2020.

Haas, F., Heckmann, T., Wichmann, V. and Becht, M.: Runout analysis of a large rockfall in the Dolomites/Italian Alps using LIDAR derived particle sizes and shapes, Earth Surf. Process. Landforms, 37, 1444–1455, https://doi.org/10.1002/esp.3295, 2012.

Heckmann, T., Bimböse, M., Krautblatter, M., Haas, F., Becht, M. and Morche, D.: From geotechnical analysis to quantification and modeling using LiDAR data: A study on rockfall in the Reintal catchment, Bavarian Alps, Germany, Earth Surf. Process. Landforms, 37, 119–133, https://doi.org/10.1002/esp.2250, 2012.

Heiser, M., Scheidl, C. and Kaitna, R.: Evaluation concepts to compare observed and simulated deposition areas of mass movements, Comput Geosci, 21, 335–343, https://doi.org/10.1007/s10596-016-9609-9, 2017.

Hergarten, S., Robl, J. and Stüwe, K.: Extracting topographic swath profiles across curved geomorphic features, Earth Surf. Dynam., 2, 97–104, https://doi.org/10.5194/esurf-2-97-2014, 2014.

Hibert, C., Mangeney, A., Grandjean, G. and Shapiro, N. M.: Slope instabilities in Dolomieu crater, Réunion island: From seismic signals to rockfall characteristics, J. Geophys. Res., 116, 1–18, https://doi.org/10.1029/2011JF002038, 2011.

Hungr, O., and Evans, S. G.: Engineering evaluation of fragmental rockfall hazards, in: Proceedings of the 5th International Symposium on Landslides, Lausanne, Switzerland, 10–15 July 1988, 685–690, 1988.

https://doi.org/10.5194/nhess-2020-322
Preprint. Discussion started: 6 October 2020
© Author(s) 2020. CC BY 4.0 License.

Jaboyedoff, M. and Derron, M.-H.: Hazard assessment within an Integrated Risk Assessment Process for Landslides (IRAPL), in: Proceedings of the International Conference on Landslide Risk Management, Vancouver, Canada, 31 May–3 June 2005, 2005.

Jaboyedoff M., Metzger R., Oppikofer T., Couture R., Derron M.-H., Locat J. and Turmel D.: New insight techniques to analyze rock-slope relief using DEM and 3D-imaging cloud points: COLTOP-3D software, in: Proceedings of the 1st Canada-US Rock Mechanics Symposium, Vancouver, Canada, 27–31 May 2007, 61–68, 2007.

Jaboyedoff, M. and Labiouse, V.: Technical note: Preliminary estimation of rockfall runout zones, Nat. Hazards Earth Syst. Sci., 11, 819–828, https://doi.org/10.5194/nhess-11-819-2011, 2011.

Jomelli, V. and Francou, B.: Comparing the characteristics of rockfall talus and snow avalanche landforms in an Alpine environment using a new methodological approach: Massif des Ecrins, French Alps, Geomorphology, 35, 181–192, https://doi.org/10.1016/S0169-555X(00)00035-0, 2000.

Kenner, R.: Mass wasting processes affecting the surface of an alpine talus slope: Annual sediment budgets 2009–2018 at Flüelapass, eastern Swiss Alps, Land Degrad Dev., 31, 451–462, https://doi.org/10.1002/ldr.3462, 2019.

Kirkby, M.J. and Statham, I.: Surface stone movement and scree formation, J Geol, 83, 349–362, www.jstor.org/stable/30059027, 1975.

Knoblich, K.: Über den Böschungswinkel von Schutthalden, Catena, 2, 1–10, https://doi.org/10.1016/S0341-8162(75)80001-4, 1975.

Kotarba, A. and Strömquist, L.: Transport, sorting and deposition processes of Alpine debris slope deposits in the Polish Tatra mountains, Geografiska Annaler: Series A, Physical Geography, 66, 285–294, https://doi.org/10.1080/04353676.1984.11880116, 1984.

Krautblatter M. and Dikau R.: Towards a uniform concept for the comparison and extrapolation of rockwall retreat and rockfall supply, Geografiska Annaler: Series A, Physical Geography, 89, 21–40, https://doi.org/10.1111/j.1468-0459.2007.00305.x, 2007.

Kromer, R., Walton, G., Gray, B., Lata, M. and Group, R.: Development and optimization of an automated fixed-location time lapse photogrammetric rock slope monitoring system, Remote Sens., 11, 1–18, https://doi.org/10.3390/rs11161890, 2019.

https://doi.org/10.5194/nhess-2020-322
Preprint. Discussion started: 6 October 2020
© Author(s) 2020. CC BY 4.0 License.

Lambert, S., Bourrier, F. and Toe, D.: Improving three-dimensional rockfall trajectory simulation codes for assessing the efficiency of protective embankments, Int J Rock Mech Min, 60, 26–36, https://doi.org/10.1016/j.ijrmms.2012.12.029, 2013.

Leine, R. I., Schweizer, A., Christen, M., Glover, J., Bartelt, P. and Gerber, W.: Simulation of rockfall trajectories with consideration of rock shape, Multibody Syst Dyn, 32, 241–271, https://doi.org/10.1007/s11044-013-9393-4, 2014.

Lénat, J.-F., Bachèlery, P. and Merle, O.: Anatomy of Piton de la Fournaise volcano (La Réunion, Indian Ocean), Bull Volcanol, 74, 1945–1961, https://doi.org/10.1007/s00445-012-0640-y, 2012.

Luckman, B. H.: Processes, transport, deposition, and landforms: rockfall, in: Mountain and Hillslope Geomorphology, Treatise on Geomorphology, edited by: Shroder, J. F., Stoffel, M. and Marston, R. A., Reference Module in Earth Systems and Environmental Sciences, 7, 174–182, https://doi.org/10.1016/B978-0-12-374739-6.00162-7, 2013a.

Luckman, B. H.: Talus slopes, edited by: Elias, S. A., The Encyclopedia of Quaternary Science, 3, 566–573, 2013b.

Meißl, G.: Modellierung der Reichweite von Felsstürzen, Fallbeispiele zur GIS-gestützten Gefahrenbeurteilung aus dem Bayerischen und Tiroler Alpenraum, Ph.D. thesis, Institute of Geography, University of Innsbruck, Austria, 249 pp., 1998.

Merle, O., Mairine, P., Michon, L., Bachèlery, P. and Smietana, M: Calderas, landslides and paleo-canyons on Piton de la Fournaise volcano (La Réunion Island, Indian Ocean), J Volcanol Geoth Res, 189, 131–142, https://doi.org/10.1016/j.jvolgeores.2009.11.001, 2010.

Messenzehl, K. and Dikau, R.: Structural and thermal controls of rockfall frequency and magnitude within rockwall-talus systems (Swiss Alps), Earth Surf. Process. Landforms, 42, 1963–1981, https://doi.org/10.1002/esp.4155, 2017.

Nappi, M., Budetta, P., Lombardi, G. and Minotta, C.: Rockfall run-out estimate comparing empirical and trajectographic approaches, in: Landslide Science and Practice Volume 6: Risk Assessment, Management and Mitigation, edited by: Margottini, C., Canuti, P. & Sassa, K., Springer, Berlin, Heidelberg, Germany, 177–182, https://doi.org/10.1007/978-3-642-31319-6_25, 2013.

Okura, Y., Kitahara, H., Sammori, T. and Kawanami, A.: The effects of rockfall volume on runout distance, Eng Geol, 58, 109–124, https://doi.org/10.1016/S0013-7952(00)00049-1, 2000.

https://doi.org/10.5194/nhess-2020-322
Preprint. Discussion started: 6 October 2020
© Author(s) 2020. CC BY 4.0 License.

Peltier, A., Bachèlery, P. and Staudacher, T.: Magma transport and storage at Piton de la Fournaise (La Réunion) between 1972 and 2007: A Review of geophysical and geochemical data, J Volcanol Geoth Res, 184, 93–108, https://doi.org/10.1016/j.jvolgeores.2008.12.008, 2009a.

Peltier, A., Staudacher, T., Bachèlery, P. and Cayol, V.: Formation of the April 2007 caldera collapse at Piton de la Fournaise volcano: Insights from GPS data, J Volcanol Geoth Res, 184, 152–163, https://doi.org/10.1016/j.jvolgeores.2008.09.009, 2009b.

Peltier, A., Villeneuve, N., Ferrazzini, V., Testud, S., Hassen, T., Boissier, P. and Catherine, P.: Changes in the long-term geophysical eruptive precursors at Piton de la Fournaise: Implications for the response management, Front. Earth Sci., 6, https://doi.org/10.3389/feart.2018.00104, 2018.

Pérez, F. L.: Talus fabric and particle morphology on Lassen Peak, California, Geografiska Annaler. Series A, Physical Geography, 71, 43–57, https://doi.org/10.2307/521007, 1989.

Pérez, F. L.: Talus fabric, clast morphology, and botanical indicators of slope processes on the Chaos Crags (California Cascades), U.S.A., Géographie physique et Quaternaire, 52, 1–22, https://doi.org/10.7202/004861, 1998.

Pfeiffer, T. J. and Bowen, T. D.: Computer simulations of rockfalls, Bulletin of the Association of Engineering Geologists, 26, 135–146, https://doi.org/10.2113/gseegeosci.xxvi.1.135, 1989.

Popescu, R., Vespremeanu-Stroe, A., Onaca, A., Vasile, M., Cruceru, N. and Pop, O.: Low-altitude permafrost research in an overcooled talus slope–rock glacier system in the Romanian Carpathians (Detunata Goală, Apuseni Mountains), Geomorphology, 295, 840–854, http://dx.doi.org/10.1016/j.geomorph.2017.07.029, 2017.

Rapp, A.: Recent development of mountain slopes in Kärkevagge and surroundings, northern Scandinavia, Geografiska Annaler, 42, 65–200, https://doi.org/10.1093/forestscience/11.1.89, 1960.

Ravanel, L., Allignol, F., Deline, P., Gruber, S. and Ravello, M.: Rock falls in the Mont Blanc Massif in 2007 and 2008, Landslides, 7, 493–501, https://doi.org/10.1007/s10346-010-0206-z, 2010.

RIEGL Laser Measurement Systems GmbH: Data Sheet, RIEGL LMS-Z420i, Horn, Austria, 2010.

RIEGL Laser Measurement Systems GmbH: Data Sheet, RIEGL VZ-4000, Horn, Austria, 2020.

https://doi.org/10.5194/nhess-2020-322
Preprint. Discussion started: 6 October 2020
© Author(s) 2020. CC BY 4.0 License.

Rixhon, G., and Demoulin, A.: Evolution of slopes in a cold climate, Treatise on Geomorphology, 8, 392–415, https://doi.org/10.1016/B978-0-12-374739-6.00218-9, 2013.

Royán, M. J., Abellán, A., Jaboyedoff, M., Vilaplana, J. M. and Calvet, J.: Spatio-temporal analysis of rockfall pre-failure deformation using Terrestrial LiDAR, Landslides, 11, 697–709, https://doi.org/10.1007/s10346-013-0442-0, 2014.

Ruiz-Carulla, R. and Corominas, J.: Analysis of Rockfalls by Means of a Fractal Fragmentation Model, Rock Mech Rock Eng, 53, 1433–1455, https://doi.org/10.1007/s00603-019-01987-2, 2020.

Sala, Z., Hutchinson, D. J., and Harrap, R.: Simulation of fragmental rockfalls detected using terrestrial laser scans from rock slopes in south-central British Columbia, Canada, Nat. Hazards Earth Syst. Sci., 19, 2385–2404, https://doi.org/10.5194/nhess-19-2385-2019, 2019.

Sanders, D., Ostermann, M. and Kramers, J.: Quaternary carbonate-rocky talus slope successions (Eastern Alps, Austria): sedimentary facies and facies architecture, Facies, 55, 345–373, https://doi.org/10.1007/s10347-008-0175-z, 2009.

Sens-Schönfelder, C., Pomponi, E. and Peltier, A.: Dynamics of Piton de la Fournaise volcano observed by passive image interferometry with multiple references, J Volcanol Geoth Res, 276, 32–45, https://doi.org/10.1016/j.jvolgeores.2014.02.012, 2014.

Serrano, E. Sanjosé, J. J., Gómez-Gutiérrez, Á. and Gómez-Lende, M.: Surface movement and cascade processes on debris cones in temperate high mountain (Picos de Europa, northern Spain), Sci Total Environ, 649, 1323–1337, https://doi.org/10.1016/j.scitotenv.2018.08.405, 2019.

Statham, I.: Scree slope development under conditions of surface particle movement, Transactions of the Institute of British Geographers, 59, 41–53, https://doi.org/10.2307/621711, 1973.

Staudacher, T., Peltier, A., Ferrazzini, V., Di Muro, A., Boissier, P., Catherine, P., Kowalski, P., Lauret, F. and Lebreton, J.: Fifteen years of intense eruptive activity (1998–2013) at Piton de la Fournaise volcano: a review, in: Active Volcanoes of the Southwest Indian Ocean. Piton de la Fournaise and Karthala, edited by: Bachèlery, P., Lénat, J.-F., Di Muro, A. and Michon, L., Springer, Berlin, Heidelberg, Germany, 139–170, https://doi.org/10.1007/978-3-642-31395-0_9, 2016.

https://doi.org/10.5194/nhess-2020-322
Preprint. Discussion started: 6 October 2020
© Author(s) 2020. CC BY 4.0 License.

Strunden, J., Ehlers, T. A., Brehm, D. and Nettesheim, M.: Spatial and temporal variations in rockfall determined from TLS measurements in a deglaciated valley, Switzerland, J. Geophys. Res. Earth Surf, 120, 1251–1273, https://doi.org/10.1002/2014JF003274, 2015.

Urai, M., Geshi, N. and Staudacher, T.: Size and volume evaluation of the caldera collapse on Piton de la Fournaise volcano during the April 2007 eruption using ASTER stereo imagery, Geophys. Res. Lett., 34, 1944–8007, https://doi.org/10.1029/2007GL031551, 2007.

Valeton, I.: Beziehungen zwischen petrographischer Beschaffenheit, Gestalt und Rundungsgrad einiger Flussgerölle (Dependencies between petrographic conditions, shape and rounding of a few bedload gravel), Petermanns Geographische Mitteilungen, 99, 13–17, 1955.

Vanneschi, C., Di Camillo, M., Aiello, E., Bonciani, F. and Salvini, R.: SfM-MVS photogrammetry for rockfall analysis and hazard assessment along the ancient Roman Via Flaminia road at the Furlo gorge (Italy), ISPRS Int. J. Geo-Inf., 8, 1–23, https://doi.org/10.3390/ijgi8080325, 2019.

Vilajosana, I., Suriñach, E., Abellán, A., Khazaradze, G., Garcia, D. and Llosa, J.: Rockfall induced seismic signals: case study in Montserrat, Catalonia, Nat. Hazards Earth Syst. Sci., 8, 805–812, https://doi.org/10.5194/nhess-8-805-2008, 2008.

Volkwein, A., Schellenberg, K., Labiouse, V., Agliardi, F., Berger, F., Bourrier, F., Dorren, L. K. A., Gerber, W. and Jaboyedoff, M.: Rockfall characterisation and structural protection-a review, Nat. Hazards Earth Syst. Sci., 11, 2617–2651, https://doi.org/10.5194/nhess-11-2617-2011, 2011.

Volkwein, A., Brügger, L., Gees, F., Gerber, W., Krummenacher, B., Kummer, P., Lardon, J. and Sutter, T.: Repetitive rockfall trajectory testing, Geosciences, 8, 1–27, https://doi.org/10.3390/geosciences8030088, 2018.

Wang, I.-T. and Lee, C.-Y.: Influence of slope shape and surface roughness on the moving paths of a single rockfall, World Academy of Science, Engineering and Technology, International Journal of Civil, Environmental, Structural, Construction and Architectural Engineering, 4, 122–128, 2010.

Wang, Y., Jiang, W., Cheng, S., Song, P. and Mao, C.: Effects of the impact angle on the coefficient of restitution in rockfall analysis based on a medium-scale laboratory test, Nat. Hazards Earth Syst. Sci., 18, 3045–3061, https://doi.org/10.5194/nhess-18-3045-2018, 2018.

https://doi.org/10.5194/nhess-2020-322
Preprint. Discussion started: 6 October 2020
© Author(s) 2020. CC BY 4.0 License.

White, S. E.: Alpine mass movement forms (noncatastrophic): Classification, description, and significance, Arctic Alpine Res, 13, 127–137, doi:10.2307/1551190, 1981.

Whitehouse, I. E. and McSaveney, M. J.: Diachronous talus surfaces in the Southern Alps, New Zealand, and their implications to talus accumulation, Arctic Alpine Res, 15, 53–64, https://www.tandfonline.com/doi/abs/10.1080/00040851.1983.12004328, 1983.

Wichmann, V.: The Gravitational Process Path (GPP) model (v1.0)-a GIS-based simulation framework for gravitational processes, Geosci. Model Dev., 10, 3309–3327, https://doi.org/10.5194/gmd-10-3309-2017, 2017.

Yamamoto, T., Takada, A., Ishizuka, Y., Miyaji, N. and Tajima, Y.: Basaltic pyroclastic flows of Fuji volcano, Japan: characteristics of the deposits and their origin, Bull Volcanol, 67, 622–633, https://doi.org/10.1007/s00445-004-0398-y, 2005.

Zevenbergen, L. W. and Thorne, C. R.: Quantitative analysis of land surface topography, Earth Surf. Process. Landforms, 12, 47–56, https://doi.org/10.1002/esp.3290120107, 1987.